ADVANCES IN PREDICTING THE NUCLEATION OF FRETTING FATIGUE CRACKS

R. W. Neu, D. R. Swalla, and J. A. Pape

The George W. Woodruff School of Mechanical Engineering
Georgia Institute of Technology
Atlanta, GA 30332-0405, USA

ABSTRACT

The nucleation of fretting fatigue cracks in a precipitation hardened stainless steel is characterized by experiments in a laboratory setting. The finite element method using an elastic-plastic material model is employed to closely simulate the experimental conditions and to determine the local cyclic response. The impact of the coefficient of friction used in the simulations is critically examined by comparing the experiments and modeling. Multiaxial fatigue criteria based on critical planes seem most appropriate for predicting fretting fatigue crack nucleation. The applicable criterion depends on the scale of the fretting fatigue process volume.

INTRODUCTION

Components that suffer from fretting fatigue damage tend to fail in the high cycle fatigue regime where globally elastic conditions prevail. Therefore, standard design analyses, whether analytical or numerical, reflect the belief that elastic material assumptions are sufficient to predict local stresses and strains where fretting fatigue cracks are likely to nucleate. These analyses often use a coefficient of friction measured from macroscopic sliding experiments or fretting under gross slip conditions. These measurements of friction are not unambiguous, especially for predicting conditions of microslip in fretting fatigue. In addition, no completely satisfactory damage model has been clearly identified, although critical plane theories for correlating multiaxial fatigue show much promise in better capturing the experimentally observed cracking [1-3].

The objectives of the current research are to better understand the fretting fatigue nucleation process in PH 13-8 Mo stainless steel as well as to develop more robust analysis tools for designing against fretting fatigue. Interrupted fretting fatigue tests are used to better understand the crack nucleation process. The robustness of the analyses may be improved by better approximating the physical processes of crack nucleation at the appropriate length scale.

EXPERIMENTS

PH 13-8 Mo is a high strength, precipitation hardened Cr-Ni stainless steel that has been used to replace AISI 4340 steel in applications where fatigue and corrosion resistance are of utmost importance. The material tested was solution treated and aged at 566°C for 4 hours. The yield and ultimate strengths are

1286 MPa and 1325 MPa, respectively, and the material is stable under cyclic loading [4]. The fatigue limit in terms of maximum stress for $R = s_{min} / s_{max} = 0.1$ loading is 930 MPa.

The fatigue specimen (19.0 mm by 3.81 mm) is clamped with a prescribed load between two bridge-type fretting pads on its edges (see Figure 1). The role of global contact geometry is studied by using pads with different shapes on each side of the fatigue specimen. For the results given here, a nominally flat pad (3 mm width) was on one side and a cylindrical pad (15 mm radius) was on the other side. The fatigue specimen, with fretting assembly attached, is then clamped into grips on a 100 kN servohydraulic fatigue test system. The fretting condition is induced by the mismatch in the cyclic strains between the fatigue specimen and the fretting pads. The frictional force is measured using a strain gage between the two contact regions on each of the fretting pads. Additional experimental details can be found in Ref. [5].

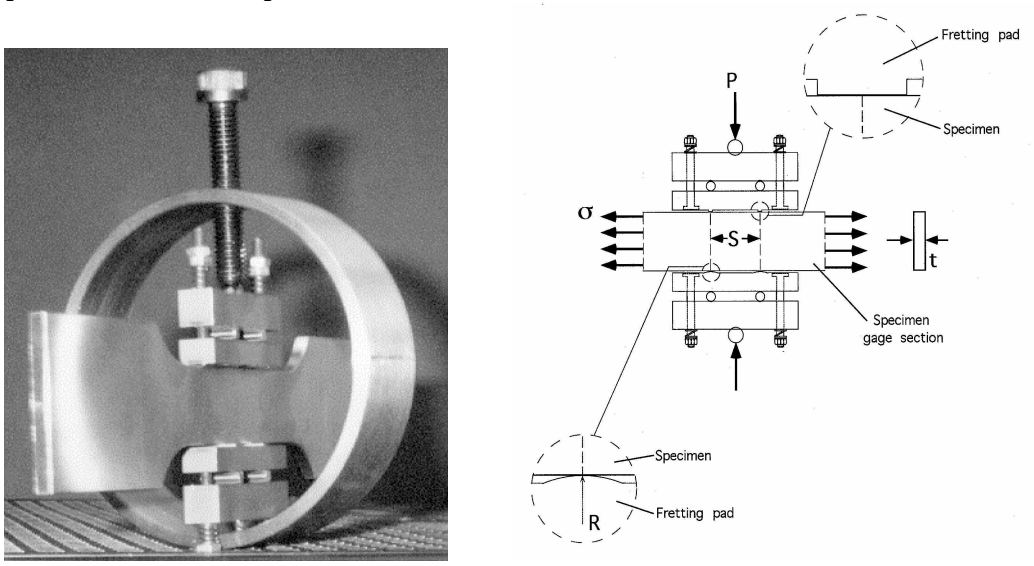

Figure 1: Fatigue specimen and fretting assembly.

This paper focuses on the results of a fatigue test conducted at R = 0.1 with a remote stress amplitude of 217 MPa and a frequency of 10 Hz. The maximum applied stress is 482 MPa, which is slightly more than one-half the "plain" fatigue limit. The normal load at each foot of the fretting pad was 343 N, which is sufficiently low to prevent yielding at a cylindrical contact based on an ideally smooth Hertzian contact analysis. However, contacting asperities will likely result in very limited yielding on the initial application of the normal load. Two tests were conducted under these conditions. The tests were stopped when a crack of about 3 mm in length was present. The cycle counts were 184,000 and 123,000. In both specimens, cracks were found at both the flat and cylindrical contacts, although the dominant crack always emanated from a foot on the cylindrical pad. Additional tests were subsequently conducted under these same conditions. These tests were interrupted at 200, 5,000, 10,000, and 100,000 cycles and then destructively examined.

Fretting scars after only 200 cycles showed patches of substantial deformation interspersed with areas where the original machining marks could be observed unaltered (see Figure 2). This is a result of asperity contact between the pads and specimen. Cracks 10-20 μm in depth appeared to surround some of the deformed patches, usually on the trailing edge of each patch (see Figure 3). By 5,000 cycles, the deformation encompassed nearly the entire fretting scar. There were still some patches where the matching marks could be observed, but they were relatively scarce. By 100,000 cycles the surface of the specimen was heavily deformed, and some major cracks could be seen. Microstructural analysis indicated a darkly etched region extending to a depth of about 50 μm below the contact by 100,000 cycles, similar to that shown at the end of the test in Figure 4 (and also seen later in Figure 8). The nature of the microstructural change in this alloy has not yet been identified. In general, these observations apply to both the cylindrical and flat contacts.

Sections through the cylindrical fretting scars at the end of the test (see Figure 4) show that initial cracks appear near the trailing edge of the contact (the sides closest to the grips). Their orientation down to a depth of 50 μm is approximately 55° as measured from the normal direction to the specimen surface. The

orientation of the crack changes as it grows deeper. At a depth of 200 μm, the crack is nearly perpendicular to the global fatigue stress direction, and consequently, the influence of the fretting force on the stress intensity is minimal when the crack reaches this depth. The cracks appear to nucleate near the boundary of the darkly etched region described previously.

The frictional force range evolved during the test as shown in Figure 5. In the initial bedding-in phase, gross slip occurs and the frictional force range, which is directly related to the coefficient of friction, increases rapidly. This generally occurs in less than 200 cycles. Then the frictional force range drops off, coinciding with the formation of microcracks on the surface (Figure 3), and eventually reaches a quasi-steady state. As a major crack grows from the fretting point, the decrease in compliance results in a drop in the frictional force range near the end of the test. In all tests, the frictional force range for the flat pad remained higher during most of the test.

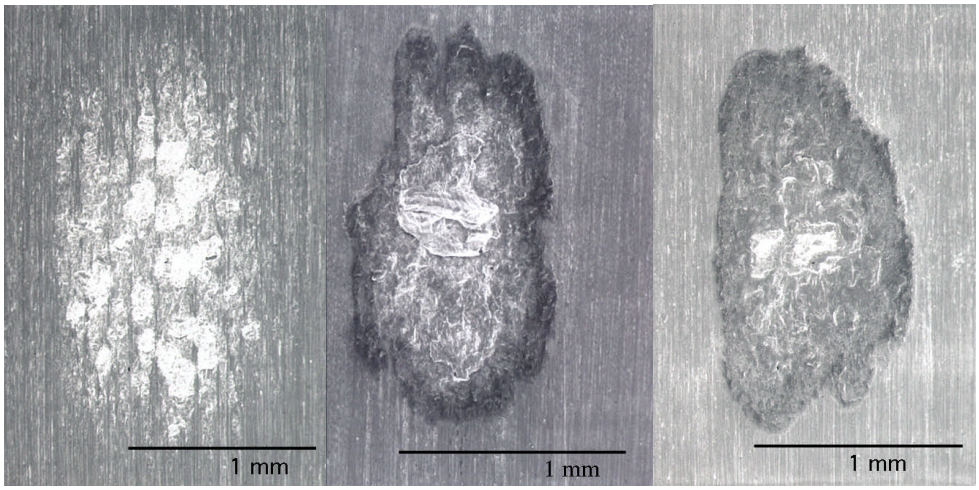

(a) 200 cycles (b) 5,000 cycles (c) 100,000 cycles

Figure 2: Fretting scars at flat contact.

Figure 3: Subsurface micrograph of flat contact at cycle 200.

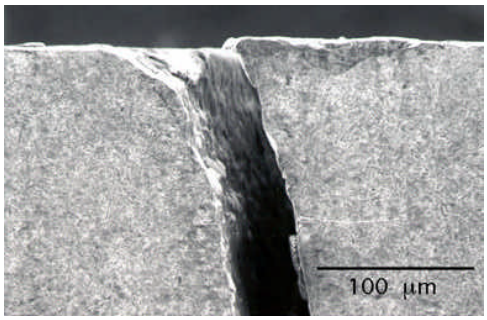

Figure 4: Subsurface micrograph at cylindrical contact at the end of the test.

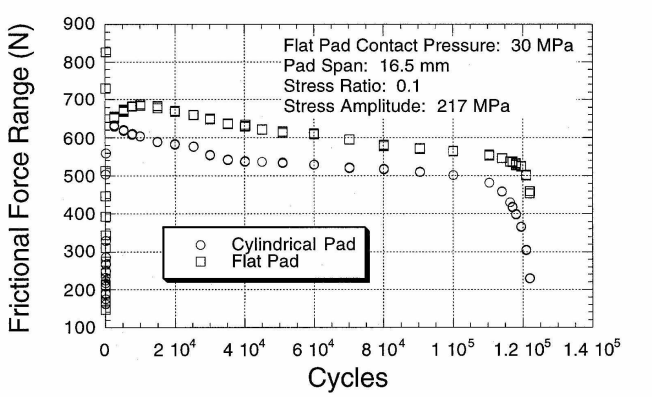

Figure 5: Evolution of frictional force range with cycles.

ELASTIC-PLASTIC FINITE ELEMENT SIMULATIONS

A 2D plane strain finite element model of the experimental conditions was developed in ABAQUS [6] as shown in Figure 6. The pad and specimen are fixed along planes of symmetry. Here, the cylindrical contact case was considered. A mapped mesh with an element width of 10 μm was used near the region of contact, and a free mesh was used elsewhere. Conditions of plane strain were considered appropriate since the area of contact is much smaller than the width of the specimen. The properties of PH 13-8 Mo are E = 192 GPa, ν = 0.3, and the plastic behavior is described using a Ziegler kinematic hardening model with nonlinear idealization of the cyclic stress-strain response (n' = 0.100 and K' = 2134 MPa). The modulus of the springy layer was set to 0.001*E. This layer provides a small constraint to eliminate rigid body motion in the early stages of the analysis [6,7]. The frictional force is not prescribed but can be determined from the reaction forces at the vertical plane of symmetry. Three full cycles were modeled by incrementing load steps during the analysis. Plastic shakedown occurred by the third cycle for the case reported. The stress-strain response of the third cycle is used in the fatigue damage analysis.

To better understand the role of the prescribed coefficient of friction (COF), the analyses were repeated using three different COF (μ = 0.75, 1.0, and 1.5). Using the frictional force range measured experimentally, the COF under gross sliding conditions near the peaks of the cycles is approximately 0.75. Here, μ = Q/P where Q is the frictional force amplitude and P is the normal load. However, as discussed later, prescribing a higher COF may provide more realistic results very locally in the contact region.

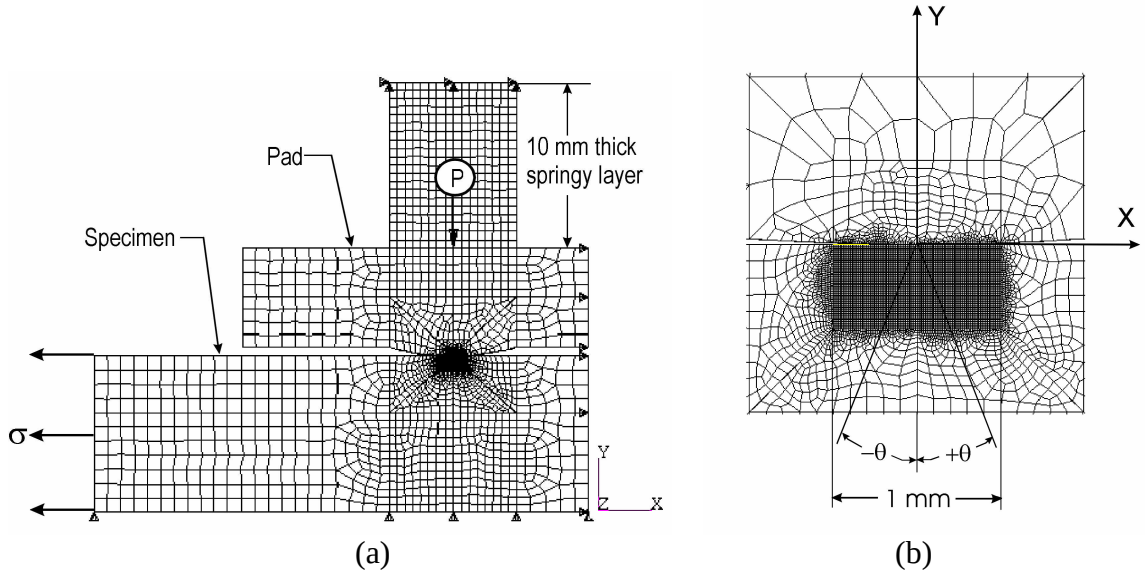

Figure 6: (a) Finite element mesh of fatigue specimen and fretting pad. (b) Mesh in loading region.

RESULTS AND DISCUSSION

The cyclic shear and tangential stresses (s_{xy} and s_{xx}, respectively) along the interface for μ = 0.75 and μ = 1.5 are shown in Figure 7. Increasing the COF increases both stress components, especially near the trailing edge of the contact (left side in these figures). When μ = 0.75, a condition of gross slip prevails at both maximum and minimum loading peaks. For μ = 1.5, a stick region prevails at the minimum peak leading to a concave region in the Δs_{xy} distribution. A higher COF better captures the stick/slip nature of the contact conditions observed experimentally [5].

The distributions of accumulated effective plastic strain after the completion of the third loading cycle are shown in Figure 8. Again, the trailing edge is on the left side. The accumulated effective plastic strain is defined as

$$e_{acc} = \int \sqrt{\tfrac{2}{3}\dot{\underset{\sim}{e}}^{p} : \dot{\underset{\sim}{e}}^{p}}\, dt \,. \qquad (1)$$

The microstructurally altered region has a shape similar to the accumulated plastic strain distribution, especially when μ = 1.5. This suggests that the higher COF captures the accumulated plastic strain distribution more effectively.

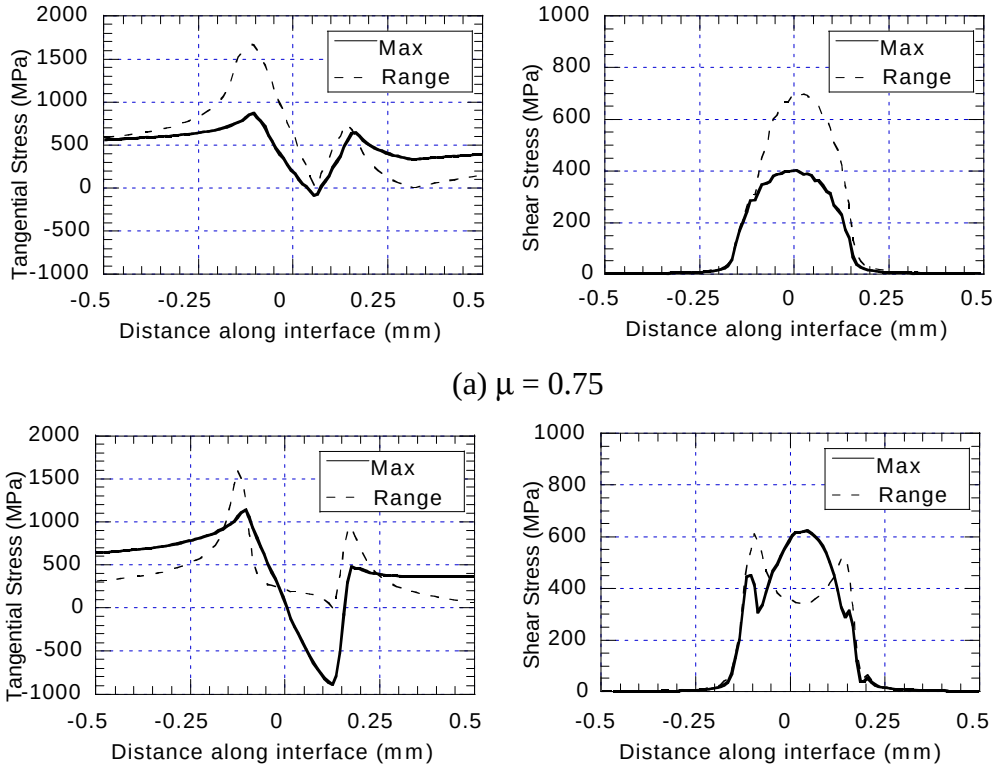

Figure 7: Maximum and range in tangential stress (s_{xx}) and shear stress (s_{xy}) along surface of fatigue specimen in the third cycle for (a) μ = 0.75 and (b) μ = 1.5.

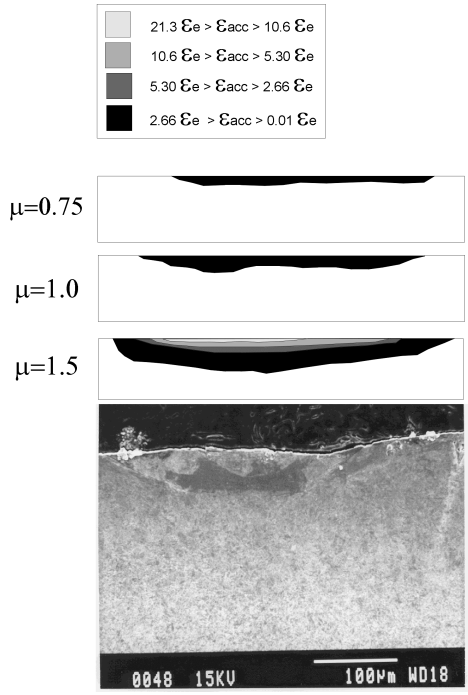

Figure 8: Contour plots of accumulated plastic strain after three cycles for different coefficients of friction, where e_e is the elastic strain at initial yielding. The micrograph is from an experiment after 100,000 cycles and is shown at the same scale as the contour plots.

By comparing the experimental results directly to the elastic-plastic analyses, it is apparent that a higher prescribed COF better represents the local conditions. There are a number of reasons why this might be the case. Real contacts consist of regions of extreme pressure and shear stress where asperities contact, and regions in between where these stresses are zero. The global normal pressure and coefficient of friction simply represent the average influence of these microscopically rough surfaces. For a global analysis, the principle of Saint-Venant is invoked, and it is fine to consider average values when values of stress and strain away from the region of contact are desired. However, for fretting fatigue, this is not a good assumption since fretting fatigue crack nucleation occurs within the region near the surface.

Another motivation for using a higher COF is the consideration that the number of asperity contacts varies with sliding position, or similarly, the globally-measured COF varies with time. Experimental results obtained from sliding tests indicate that the near instantaneous globally-measured COF can vary anywhere from 0.1 to as high as 2.0 [8]. The temporal probability distribution of these experimental results most closely fits a gamma function, as illustrated in Figure 9. The spatial distribution is likely to have an even larger range, including a large peak at $\mu = 0$, representing areas of no contact between asperities, and near infinity for regions of local welding. The influence of this nonuniform COF is likely to become greater as the size of the global contact is reduced. The extreme values of the distribution function likely play a more important role in capturing the long-term steady-state behavior than using the mean value, which is the one typically reported and used in analyses. Therefore, friction models that predict a single value of friction, and not a spatial or temporal distribution of friction values, may not be representative of actual conditions very near the contact. Using a mean value of COF is analogous to conducting a stress analysis and not considering the influence of notches in raising the stress and strain concentration.

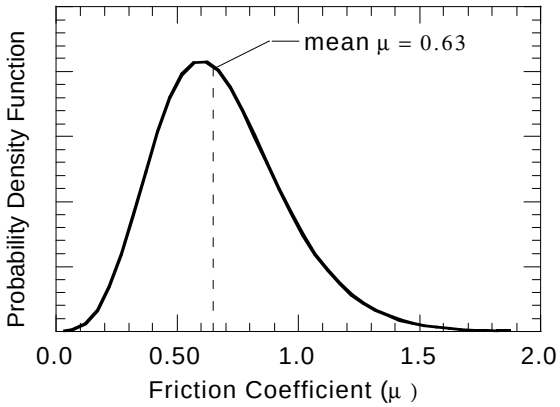

Figure 9: Temporal distribution of the friction coefficient based on experiments found in Ref. [8].

A higher value of COF is found to give more representative results of deformation in the region near the surface [9]. A higher COF artificially simulates the influence of local stress concentration mechanisms that are nearly impossible to duplicate in a structural scale analysis. One source of stress concentration is generated by local adhesion. Another source is the stress field produced at an asperity wedge. A third source is the stress field that extends around the Mode II microcrack tips that form very early during cycling, as shown in Figure 3 [9]. Presently, the direct influence of these stress concentration mechanisms are neglected in smooth contact analyses. These stress concentration mechanisms likely play an important role in increasing both the depth of penetration of cyclic plastic deformation as well as cumulative flow near the surface [9]. By using a higher COF in the smooth contact analysis, the influence of a lower length scale is approximated without having to consider actual asperities or microcracks, which would be computationally expensive for structural analyses.

Once a structural analysis has been performed, the fretting fatigue damage can be predicted using a critical plane theory of multiaxial fatigue. Critical plane theories are meaningful from a physical argument based on the observation that cracks grow along planes in a preferred orientation relative to the cyclic stress state. A critical plane theory hypothesizes that fatigue life is dependent on the cyclic stress-strain response resolved on a plane, with the critical plane being the one that experiences the largest damage. A common shear-based critical plane parameter for strain-controlled conditions is the Fatemi-Socie (F-S) parameter [10]. The

postulate of this criterion is that the fatigue damage is dependent on the maximum cyclic shear strain amplitude on the critical plane, with damage being amplified by the level of the maximum normal stress experienced on this plane, $s_{n,\max}$. The fatigue damage – life relationship can be described by

$$\frac{\Delta g}{2}\left(1+k\frac{s_{n,\max}}{s_y}\right)=\frac{t_f'}{G}(2N_i)^{b_o}+g_f'(2N_i)^{c_o} \tag{2}$$

where N_i is the number of cycles to nucleate a crack of a certain size. The right-hand side of this equation is a fit to experimental fatigue data under cyclic shear, or if that is not available, these constants can be approximated using uniaxial data and a von Mises assumption.

Crack nucleation likely occurs from repeated reversals of dislocation slip along preferential slip planes near the fretting fatigue contact. A critical plane approach that may better describe this process is based on the vacancy-dislocation-dipole model of Mura and Nakasone [11]. The critical plane for this model is the one experiencing the largest shear strain amplitude averaged over an appropriate length, which is generally smaller than that considered in the application of the Fatemi-Socie parameter. This intrinsic length appears to range in the neighborhood of 5 μm [12] to 20 μm [2]. For the dislocation-dipole model the normal stress has less influence compared to that predicted by the Fatemi-Socie parameter.

There are two planes in an elementary volume that experience the largest shear strain range. Of these two planes, one is oriented close to 60° in the region of maximum damage near the trailing edge (see Figure 6 for angle convention), and is nearly parallel to the contours of constant accumulated plastic strain as shown in Figure 8. The other plane is oriented near -30° and is in a direction where there is a steep decreasing gradient in the constant accumulated plastic strain contours. Therefore, when the cyclic shear strain is averaged over these two planes, the 60° plane experiences a larger reverse slip over a given length. The 60° plane is consistent with the initial orientation of fretting fatigue cracks observed experimentally.

The applicable critical plane multiaxial fatigue criterion depends on the scale of the crack nucleus. For very small crack nuclei (order of 10 μm), a criterion based on a dislocation-dipole model may be appropriate. For larger cracks (order of 100 μm), a Fatemi-Socie parameter (Eqn. 2) is likely more predictive. For engineering crack nuclei (order of 1 mm), a Smith-Watson-Topper parameter may closely approximate the average influences of the cyclic stress and strain on crack formation and early growth for tensile-cracking materials [1,10]. A Fatemi-Socie parameter may still be appropriate for materials dominated by shear-cracking [10]. Microstructure plays an important role in the transition between these regimes and therefore the range in applicability of each criterion. Because of this scaling, the cyclic stress and strain behavior needs to be averaged on a plane over the appropriate length, especially in the region very close to the contact interface where the gradients in stress and strain are significant [2,12,13]. Experiments also indicate that a length scale must enter into the problem for predicting a fretting fatigue threshold [13].

Multiaxial fatigue criteria that are based on stress averages within an elementary volume at the microscopic or mesoscopic scale may also be appropriate [14,15]. These more traditional multiaxial fatigue criteria aimed at plain fatigue consider an elementary volume that contains several grains of different crystallographic orientation, so they may be more appropriately applied when considering an intermediate scale (order of 100 μm) or "large" scale (order of 1 mm). The minimum size of the fretting fatigue process volume may also be related to the microstructural dimension such as grain size. Some recent work modeling individual grains using crystal plasticity in a finite element analysis of fretting fatigue is currently being conducted to study this and related issues [16].

CONCLUSIONS

Under fretting fatigue conditions that lead to failure in more than 100,000 cycles in PH 13-8 Mo stainless steel, multiple cracks around 10 to 20 μm in length nucleate in less than 200 cycles. This cracking manifests itself as a drop in the frictional force range as compliance of individual asperities changes locally.

The effective local coefficient of friction (COF) is greater than that measured under macroscopic gross sliding conditions. A higher COF better accounts for the stress concentrations resulting from asperity interactions, adhesion, and microcrack tip stress fields. A higher COF leads to cumulative plastic strain distributions and stick/slip conditions more representative of those observed experimentally.

The applicable critical plane multiaxial fatigue criterion for fretting fatigue conditions depends on the scale of the fretting fatigue process volume. Three scales were identified.

ACKNOWLEDGMENTS

This work was funded by the Office of Naval Research through grants N00014-95-1-0539 and N00014-98-1-0532.

REFERENCES

1. Szolwinski, M.P. and Farris, T.N. (1996) *Wear* **198**, 93.
2. Lamacq, V., Dubourg, M.-C., and Vincent, L. (1997) *Tribology Int.* **30**, 391.
3. Neu, R.W., Pape, J.A., and Swalla, D.R. (2000). In: *Fretting Fatigue: Current Technology and Practices, ASTM STP 1367*, D.W. Hoeppner, V. Chandrasekaran, and C.B. Elliott, Eds., pp. 369-388.
4. Patel, A.M., Neu, R.W., and Pape, J.A. (1999) *Met. Mater. Trans. A* **30A**, 1289.
5. Pape, J.A. and Neu, R.W. (1999) *Wear* **225-229**, 1205.
6. ABAQUS (1998) version 5.8, Hibbitt, Karlsson and Sorensen, Inc., Pawtucket, RI, USA.
7. McVeigh, P.A. and Farris, T.N. (1997) *J. of Tribology* **119**, 797.
8. Blau, P. (1996). *Friction Science and Technology*. Marcel Dekker, New York.
9. Hughes, D.A., Dawson, D.B., Korellis, J.S., and Weingarten, L.I. (1994) *J. Mat. Engng. Perform.* **3**, 459.
10. Socie, D.F. (1993). In: *Advances in Multiaxial Fatigue, ASTM STP 1191*, D.L. McDowell and R. Ellis, Eds., pp. 7-36.
11. Mura, T. and Nakasone, Y. (1990) *J. Appl. Mech.* **57**, 1.
12. Fouvry, S., Kapsa, P., and Vincent, L. (2000). In: *Fretting Fatigue: Current Technology and Practices, ASTM STP 1367*, D.W. Hoeppner, V. Chandrasekaran, and C.B. Elliott, Eds., pp. 167-182.
13. Nowell, D., Hills, D.A., and Moobola, R. (2000). In: *Fretting Fatigue: Current Technology and Practices, ASTM STP 1367*, D.W. Hoeppner, V. Chandrasekaran, and C.B. Elliott, Eds., pp. 141-153.
14. Ballard, P., Dang Van, K., Deperrois, A., and Papadopoulos, Y.V. (1995) *Fatigue Fract. Engng. Mater. Struct.* **18**, 397.
15. Papadopoulos, I.V., Davoli, P., Gorla, C., Filippini, M., and Bernasconi, A. (1997) *Int. J. Fatigue* **19**, 219.
16. Goh, C.-H., Wallace, J.M., Neu, R.W., and McDowell, D.L. (2000). In: proc. 5th National Turbine Engine High Cycle Fatigue Conf., Chandler, AZ, USA, 7-9 March 2000.